Ultramicroscopy 200 (2019) 79–83

Contents lists available at ScienceDirect

Ultramicroscopy

journal homepage: www.elsevier.com/locate/ultramic

Selected energy dark-field imaging using low energy electrons for optimal surface phase discrimination

Y.R. Niu*, J. Pereiro, D. Gomez, D.E. Jesson

School of Physics and Astronomy, Cardiff University, Cardiff, CF24 3AA, United Kingdom

ARTICLE INFO

Keywords:
LEEM
Dark-field
GaAs
Surface phase

ABSTRACT

We propose a general strategy for surface phase discrimination by dark-field imaging using low energy electrons, which maximizes contrast using diffraction spots, at selected optimal energies. The method can be automated to produce composite phase maps in real space and study the dynamics of complex phase transformations in real-time. To illustrate the capabilities of the technique, surface phases are mapped in the vicinity of liquid Ga droplets on the technologically important GaAs (001) surface.

1. Introduction

Low energy electron microscopy (LEEM) is a powerful technique for imaging surface dynamic phenomena in real-time and the technique is described in detail in a number of excellent reviews [1,2] and texts [3]. The key to LEEM operation is that the specimen surface of interest forms part of an immersion lens and is maintained at a potential close to that of the electron source. A uniform electric field between the objective lens anode and the sample surface decelerates the incident electrons to an energy controlled by the bias between the specimen and the electron source potential. Typically, this is of the order of several electron volts. Following the low energy interaction and reflection from the sample surface, the electrons are re-accelerated to the gun energy on their return to the objective lens. For crystalline surfaces, a low energy electron diffraction (LEED) pattern is formed in the back focal plane of the objective lens. After transfer to the imaging column via the magnetic sector field, the diffraction pattern is reproduced at a conjugate plane to the back focal plane via a transfer lens. An image is then formed by selecting one of these diffracted beams using a contrast aperture located in this plane. If the specular beam is selected, this is termed bright-field imaging. Imaging with non-specular beams is referred to as dark-field imaging. The imaging column optics can be adjusted to produce a magnified image on the microchannel plate/phosphor screen detector. Alternatively, the optics can be adjusted to image the diffraction pattern.

Typically, LEEM dark-field imaging is applied at constant incident beam energy. This has been used to discriminate between numerous surface reconstructions [1–10]. The difference in I(V) curves (i.e. diffracted intensity against incident beam energy or bias), even for the specular (00) beam, has also readily allowed the identification between (7×7) and (1×1) domains at constant energy [11]. However, with complex surfaces exhibiting varying stoichiometry, such as GaAs (001), the diffraction information itself and hence, dark-field images, can be highly misleading at a given energy. Consider, for example, the two LEED patterns obtained from GaAs (001) at differing incident beam energies contained in Fig. 1. The first pattern at 10.6 eV displays a (4×1) periodicity. However, at 6.6 eV the pattern displays a $c(8 \times 2)$ periodicity. This simple case illustrates that one must scan the LEED pattern across a range of incident beam energy to determine the highest periodicity of the surface structure. This is further complicated in some GaAs (001) reconstructions where, for a $(l \times n)$ periodicity, not all diffracted orders in the LEED pattern are visible at a single energy, making an incident energy scan essential for accurate characterisation. In some cases, LEED spots from different phases can also overlap and it is necessary to select energies to optimise phase discrimination (see Section 3). For these reasons, it is therefore necessary to establish a strategy to distinguish phases on complex surfaces based on I(V) measurements, which is explored in the following section.

2. Selected energy dark-field LEEM

To illustrate the use of selected energy dark-field (SEDF) imaging to optimise surface phase discrimination in LEEM, we focus on the GaAs (001) surface. Experiments were carried out with a commercial ELMITEC LEEM instrument specially modified to study the III-V system [12,13]. This includes the incorporation of an As cracker source and an integrated liquid nitrogen cooling shroud to control the As background pressure in the chamber. The base pressure of the microscope is in the

* Corresponding author. Current address: MAX IV Laboratory, Lund University, PO Box 118, SE-221 00, Lund, Sweden
E-mail address: yuran.niu@maxlab.lu.se (Y.R. Niu).

https://doi.org/10.1016/j.ultramic.2019.02.017
Received 14 December 2018; Accepted 18 February 2019
Available online 19 February 2019

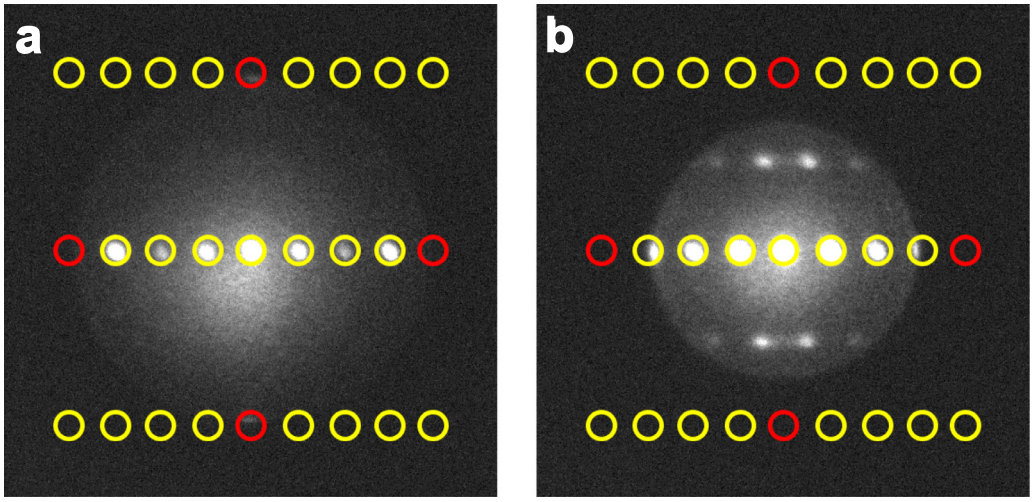

Fig. 1. LEED patterns of the c(8 × 2) surface reconstruction at (a) 10.6 eV and (b) 6.6 eV. The apparent (4 × 1) periodicity in (a) is misleading. (1,0) and (0,1) type spots are indicated by red circles. (1, *n*) and ($\bar{1}$, *n*) rows of spots lie outside the Ewald sphere and are represented by yellow circles.

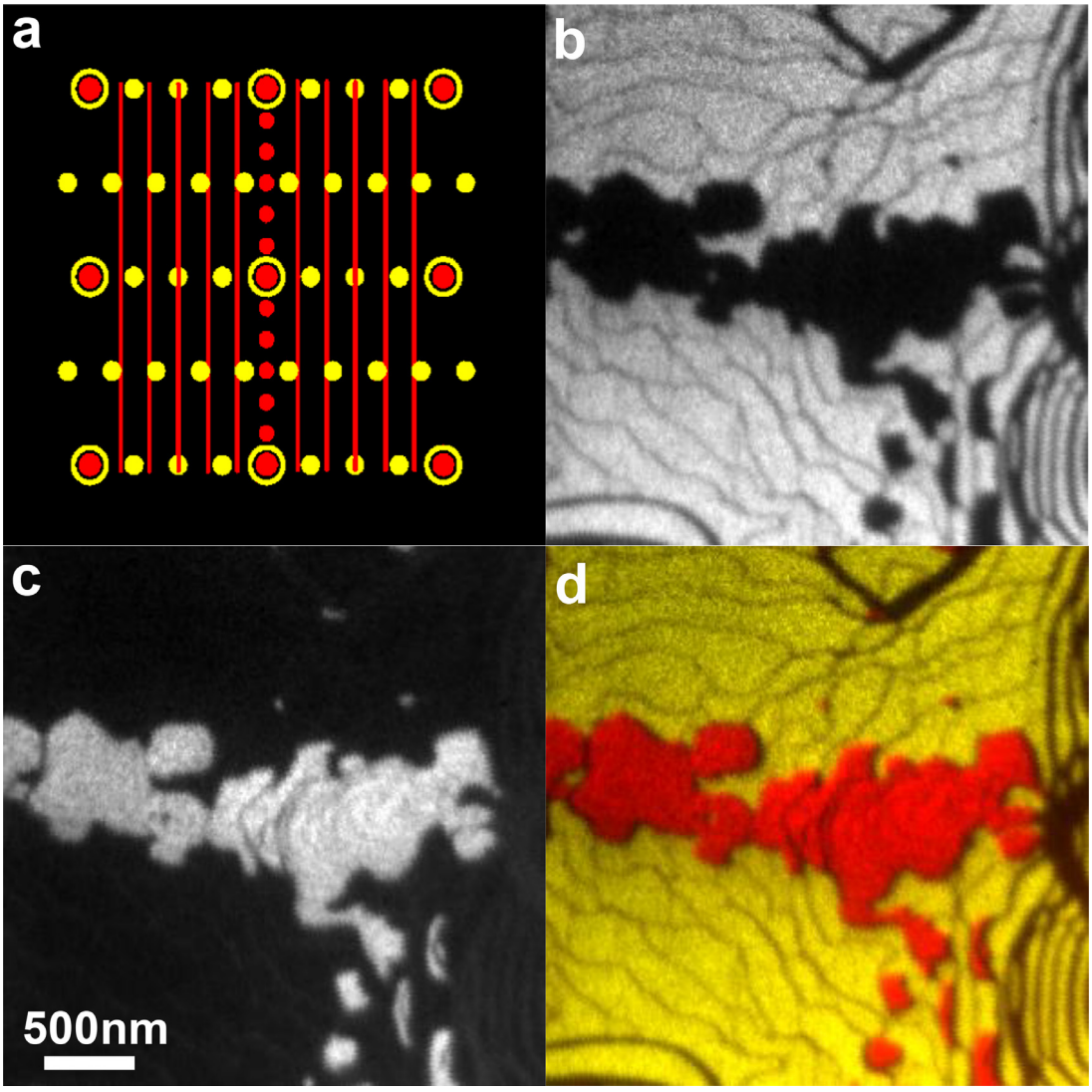

Fig. 2. (a) Schematic superimposition of c(8 × 2) (yellow) and (6 × 6) (red) LEED patterns. (b) Dark-field image of the c(8 × 2) phase obtained with the (1/4, 0) spot at 6.2 eV (see Fig. 3(a)). (c) Dark-field image of the (6 × 6) phase obtained with the (0, 3/6) spot at 5.0 eV (see Fig. 3(c)). (d) Composite SEDF LEEM image obtained by assigning yellow to the dark-field c(8 × 2) intensity in 2(b) and red to (6 × 6) intensity in 2(c). (For interpretation of the references to colour in this figure legend, the reader is referred to the web version of this article.)

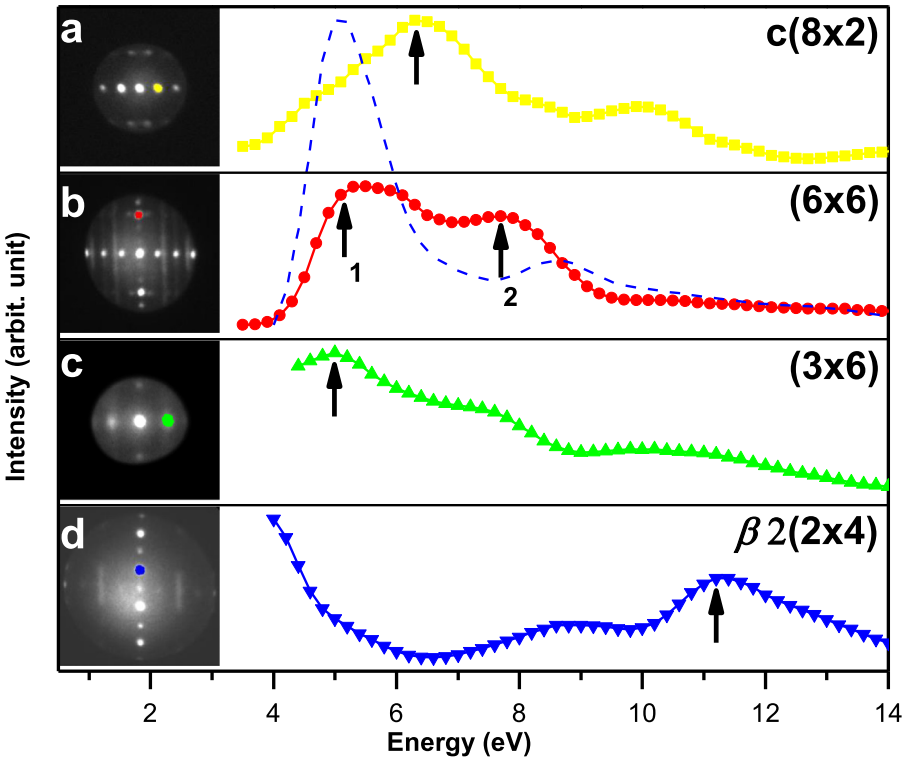

Fig. 3. I(V) curves for selected diffraction spots highlighted by colours in the LEED pattern insets. (a) (1/4, 0) spot of c(8 × 2), (b) (0, 3/6) spot of (6 × 6), (c) (1/3, 0) spot of (3 × 6) and (d) (0, 1/4) spot of β2(2 × 4). The LEED patterns are obtained at the optimal energies indicated by the black arrows under the I(V) curves (arrow 1 in panel (b)). In (b) the blue dashed curve corresponds to the (0, 2/4) spot of β2(2 × 4). (For interpretation of the references to colour in this figure legend, the reader is referred to the web version of this article.)

low 10^{-10} Torr regime. During As deposition, the pressure increases to higher 10^{-8} Torr and the beam equivalent pressure (BEP) of As flux is typically 10^{-7} Torr. The initial planar c(8 × 2) surface is obtained via a well-developed technique by running the Ga droplets over a rough GaAs (001) surface following oxide desorption [14–16]. This is described in detail in [16] but, briefly, the Ga droplets are produced by heating the sample above the congruent temperature at 650 °C. The temperature is then lowered to just below the congruent evaporation temperature (~590 °C) and droplets are allowed to run across the surface [14]. Planar c(8 × 2) trails are then left behind the droplets and are the regions used for imaging. The droplets can also be removed by annealing the sample at about 570 °C when required [16]. The GaAs sample is held firmly against a support ring by a Mo cap. A W/Re3%–W/Re25% thermocouple, spot-welded to the support ring, is used for temperature calibration in combination with infrared pyrometry.

To illustrate the principle of SEDF LEEM, we consider the relatively simple case of discriminating between (6 × 6) and c(8 × 2) phases. Coexistence between these two phases is obtained by removing droplets from the surface by annealing and then reducing the temperature to 530 °C [15]. Fig. 2(a) contains a schematic of the superimposed LEED pattern of the (6 × 6) and c(8 × 2) phases. Clearly, there are several reflections which can be used to differentiate between the two phases using dark-field imaging. Here we select the (1/4, 0) spot of the c(8 × 2) phase highlighted in yellow on the LEED pattern inset contained in Fig. 3(a). For this spot, the electron energy can be optimised to provide significant intensity. The intensity of this spot as a function of incident electron beam energy, the so-called I(V) curve, is also shown in Fig. 3(a). The optimum choice of energy to maximise the intensity is illustrated by the arrow and occurs at 6.2 eV. The resulting (1/4, 0) dark-field LEEM image for this optimum energy is contained in Fig. 2(b). Similarly, the (0, 3/6) beam for the (6 × 6) reconstruction and its associated I(V) curve is contained in Fig. 3(b). The optimum energy is 5.0 eV, as illustrated by arrow 1 in Fig. 3(b) and the resulting (0, 3/6) dark-field LEEM image is contained in Fig. 2(c). Note that the optimum energy for the (0, 1/6) spot is approximately 11 eV (not shown), but this reflection is much less intense than that of the (0, 3/6) spot. The dark-field images in Fig. 2(b) and (c) can be combined in a single composite image by assigning different colors to the intensities from the two phases. In this case we assign yellow to c(8 × 2) and red to (6 × 6) giving the composite SEDF LEEM image contained in Fig. 2(d). This contains all the information present in the two original dark-field images and provides an efficient means of visualising the coexisting phases on the surface. We note that since the contrast aperture only allows the signal from selected phases, the intensity on the detector from non-selected phases is in principle zero (neglecting inelastic scattering). Compared with conventional bright-field imaging, which can also show contrast between two phases at an optimized energy, this is likely to provide much higher contrast.

3. SEDF LEEM of droplet epitaxy on GaAs (001)

Droplet epitaxy [17] has emerged as a flexible technique for controlling the morphology of quantum structures [18–24] including double-dots [18], molecules [19], rings [20] and multi-rings [21–24]. In this approach, liquid metal droplets are first deposited on a semiconductor surface. Then exposure to a group-V flux results in the formation of a crystalline epitaxial quantum structure. Here we apply SEDF LEEM to identify surface phases surrounding liquid Ga droplets on GaAs (001) under As flux.

During droplet epitaxy on GaAs (001), we find that (3 × 6) and β2(2 × 4) reconstructions also occur in addition to the c(8 × 2) and (6 × 6) phases. A full discussion of these surface phases and their relationship to the GaAs (001) phase diagram is provided in [15,25,26] and references contained therein. The c(8 × 2) and (6 × 6) phases are known to be Ga-rich [15,25] and the β2(2 × 4) phase is As-rich [25]. The LEED I(V) curve for the (1/3, 0) reflection of the (3 × 6) phase is shown in Fig. 3(c). Similarly, the I(V) curve for the (0, 1/4) reflection of the β2(2 × 4) reconstruction is contained in Fig. 3(d). The arrows under the LEED I(V) curves in panels 3(c) and 3(d) indicate the optimal imaging energies as 5.0 and 11.2 eV.

To discriminate between the phases we must also note the complication that the (0, 2/4) spot of β2(2 × 4) is at the same reciprocal space (momentum) position as (0, 3/6) of (6 × 6) (panel 3(c)). The LEED I(V)

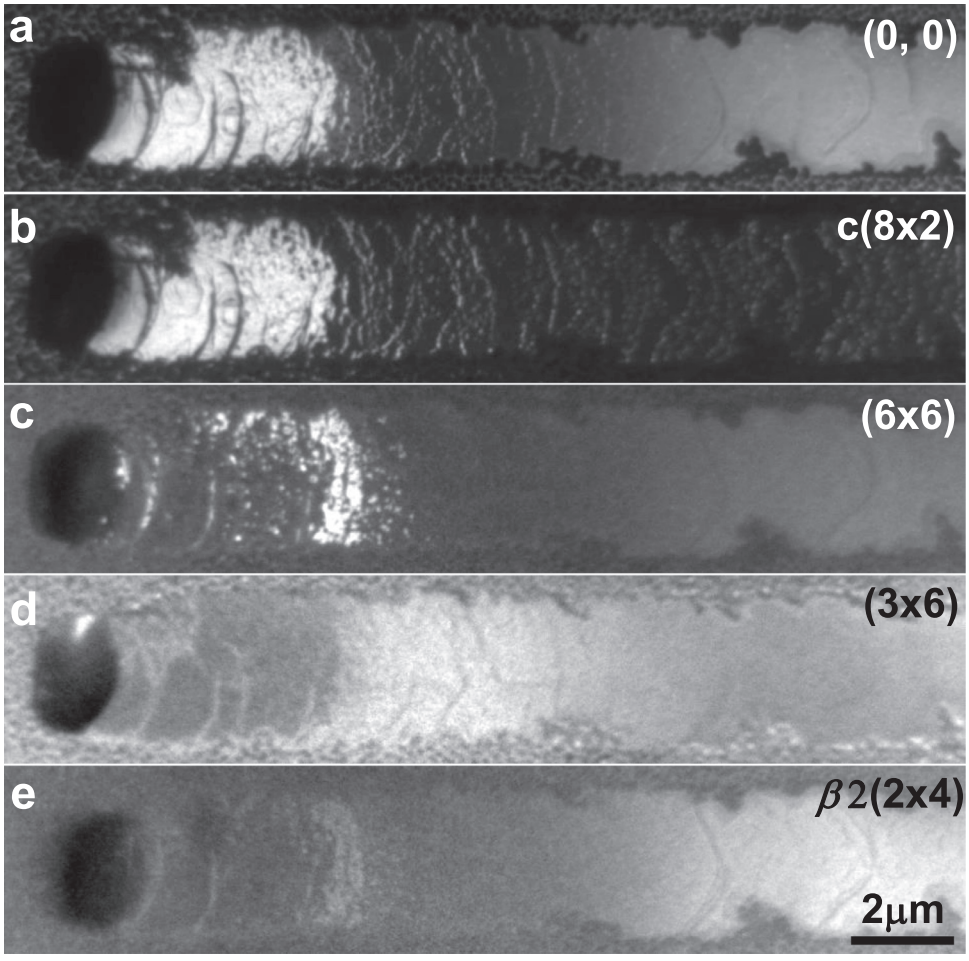

Fig. 4. LEEM images of a droplet trail on GaAs (001) after exposing to As flux for 1500 s: (a) bright-field image obtained at 8.6 eV. Dark-field images obtained with (b) the (1/4, 0) spot of c(8 × 2), (c) the (0, 3/6) spot of (6 × 6), (d) the (1/4, 0) spot of (3 × 6) and (e) the (0, 1/4) spot of β2(2 × 4). The dark-field images are obtained at the optimal energies indicated by the arrows under the I(V) curves in Fig. 3 (arrow 2 in panel(b)).

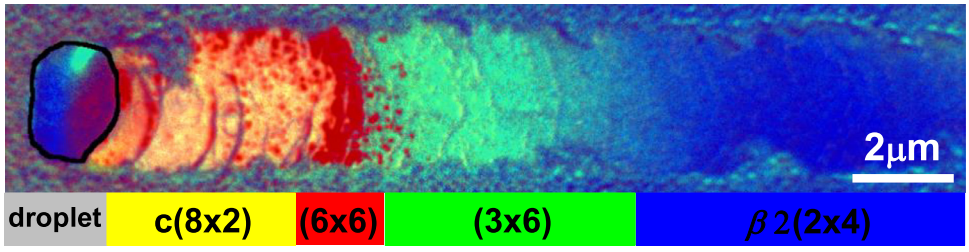

Fig. 5. Composite SEDF LEEM image formed by respectively assigning the colours yellow, red, green and blue to the intensities of the c (8 × 2), (6 × 6), (3 × 6) and β2(2 × 4) dark-field images contained in Fig. 4(b)–(e). Note the irregular shape of the droplet is due to contact line pinning. (For interpretation of the references to colour in this figure legend, the reader is referred to the web version of this article.)

curves of the (0, 2/4) spot is superimposed as the blue dashed line in panel 3(b). Clearly, the use of 5 eV (arrow 1 in panel 3(b)) for the (0, 3/6) reflection will also include a large contribution from β2(2 × 4). To avoid this, we use the next optimized energy of the (0, 3/6) dark-field image of the (6 × 6) phase indicated by arrow 2 in panel 3(b). Here, the intensity of the (0, 2/4) reflection is much lower than that of (0, 3/6). In principle, we might alternatively use (0, 1/6) to avoid overlap with (0, 2/4), but, in this case, the intensity of (0, 1/6) is too low for imaging, even at its optimum energy. Additionally, the position of (0, 1/6) is close to the (0, 1/4) spot used for imaging the β2(2 × 4) phase so that small misalignments of the contrast aperture could still mix dark-field signals from the two phases. We therefore use the (0, 3/6) spot at 7.7 eV for (6 × 6) (arrow 2, panel 3(b)) and the (0, 1/4) spot at 11.2 eV for β2(2 × 4) (arrow in panel 3(e)).

With the optimised parameters for the four surface reconstructions (Fig. 3), we can program the microscope's control software to automatically attain a sequence of optimal dark-field images for the four phases [27]. Since the LEEM images are measured at different electron energies, the current offsets of the objective lens have to be pre-programmed for the recording of image sequences, due to chromatic aberration. A sequence of one bright and four dark-field images is typically attained in several seconds, which is considerably faster than the rate of surface phase transformations for our deposition conditions. Consequently, we can study droplet epitaxy with temporally resolved SEDF LEEM.

Fig. 4(a) displays a bright-field image of a droplet and smooth surface trail following exposure to As flux for 1500 s. The trail had been formed previously by droplet motion [14] at 590 °C before the exposure to the As flux. This technique has been usefully applied to create smooth GaAs surface regions for surface science studies [16]. Panels 4(b)–(e) show the corresponding dark-field images for the c(8 × 2), (6 × 6), (3 × 6) and β2(2 × 4) phases obtained using selected

diffraction spots at optimal energies, as discussed earlier (see Fig. 3). It can be seen that the phases are located in different spatial regions of the trail. Here, the droplet under As flux is stationary, but the phase boundaries are slowly moving towards the droplet from right to left (~0.4 μm/min.). The order of the observed phases reflects the Ga adatom concentration profile (i.e. the Ga chemical potential) which decreases with distance away from the droplet. Hence, the order of the phases is consistent with existing knowledge of the GaAs phase diagram [15,25,26] and the Ga-rich or As-rich nature of the phases, as discussed earlier. Note that the (6 × 6) phase occupies a narrow spatial band located approximately 4 μm form the droplet edge. Interestingly, this cannot be distinguished in the bright-field image (panel 4(a)) because the (0, 0) I(V) curves of the (3 × 6) and (6 × 6) phases (not shown) are very similar.

As with Fig. 2(d), we can form the composite SEDF LEEM image by respectively assigning the colours yellow, red, green and blue to the intensities of the c(8 × 2), (6 × 6), (3 × 6) and β2(2 × 4) phases contained in Fig. 4(b)–(e). Since the time taken to obtain the sequence of images in Fig. 4 is 12.6 s, which is fast compared to phase boundary motion, the resulting image in Fig. 5 can be regarded as an instantaneous snapshot of the surface phase distribution under As flux, surrounding the droplet. This temporally resolved spatial phase distribution, made visible by SEDF LEEM, provides a new basis for studying the surface thermodynamics of GaAs (001) reconstructions and related phase transformation mechanisms.

4. Conclusions

We have proposed, and experimentally demonstrated, the technique of SEDF LEEM for phase discrimination on complex surfaces of varying local structure and stoichiometry. Composite images are created by combining dark-field images for each phase formed by selecting diffracted beams at optimal energies to maximise contrast. The optimal selection of the diffracted beams and energies is based on the measurement of I(V) curves. We have applied this method to investigate the surface phase distribution around liquid Ga droplets on GaAs (001) under As flux. The strategy and methods presented here are quite general and should be applicable to the characterisation of complex surfaces and study of phase transformation dynamics across a wide range of materials systems.

Acknowledgements

The authors acknowledge support from EPSRC research grant nos. EP/P023452/1 and EP/N022661/1. This project also has received funding from the European Union's Horizon 2020 research and innovation programme under the Marie Skłodowska-Curie grant agreement no. 701246. Information on the data that underpins the results presented here, including how to access them, can be found in the Cardiff University data catalogue at http://doi.org/10.17035/d.2019.0069660004.

References

[1] E. Bauer, Low energy electron microscopy, Rep. Prog. Phys. 57 (1994) 895–938 https://doi.org/10.1088/0034-4885/57/9/002.
[2] M.S. Altman, Trends in low energy electron microscopy, J. Phys. Condens. Matter 22 (2010) 084017 https://doi.org/10.1088/0953-8984/22/8/084017.
[3] E. Bauer, Surface microscopy with low energy electrons, Springer, New York, 2014https://doi.org/10.1007/978-1-4939-0935-3.
[4] R.M. Tromp, M.C. Reuter, Step morphologies on small-miscut Si(001) surfaces, Phys. Rev. B 47 (1993) 7598–7601 https://doi.org/10.1103/PhysRevB.47.7598.
[5] E. Hilner, A.A. Zakharov, K. Schulte, P. Kratzer, J.N. Andersen, E. Lundgren, A. Mikkelsen, Ordering of the nanoscale step morphology as a mechanism for droplet self-propulsion, Nano. Lett. 9 (2009) 2710–2714 https://doi.org/10.1021/nl9011886.
[6] K.L. Man, Q. Guo, M.S. Altman, Growth and oxidation of Cr films on the W(100) surface, Surf. Sci. 600 (2006) 1060–1070 https://doi.org/10.1016/j.susc.2005.12.030.
[7] L. Gao, W. Ren, H. Xu, L. Jin, Z. Wang, T. Ma, L.P. Ma, Z. Zhang, Q. Fu, L.M. Peng, X. Bao, H.M. Cheng, Repeated growth and bubbling transfer of graphene with millimetre-size single-crystal grains using platinum, Nat. Commun. 3 (2012) 699 https://doi.org/10.1038/ncomms1702.
[8] H. Marchetto, T. Schmidt, U. Groh, F.C. Maier, P.L. Lévesque, R.H. Fink, H.J. Freund, E. Umbach, Direct observation of epitaxial organic film growth: temperature-dependent growth mechanisms and metastability, Phys. Chem. Chem. Phys. 17 (2015) 29150–29160 https://doi.org/10.1039/C5CP05124J.
[9] T.A. de Jong, E.E. Krasovskii, C. Ott, R.M. Tromp, S.J. van der Molen, J. Jobst, Intrinsic stacking domains in graphene on silicon carbide: a pathway for intercalation, Phys. Rev. Mater. 2 (2018) 104005 https://doi.org/10.1103/PhysRevMaterials.2.104005.
[10] M. Soldemo, Y.R. Niu, A. Zakharov, E. Lundgren, J. Weissenrieder, A well-ordered surface oxide on Fe(110), Surf. Sci. 639 (2015) 13–19 https://doi.org/10.1016/J.SUSC.2015.04.008.
[11] W. Telieps, E. Bauer, The (7 × 7) ↔ (1 × 1) phase transition on Si(111), Surf. Sci. 162 (1985) 163–168 https://doi.org/10.1016/0039-6028(85)90890-8.
[12] D.E. Jesson, W.X. Tang, Surface electron microscopy of Ga droplet dynamics on GaAs (001), Microsc. Sci. Technol. Appl. Educ. (2010) 1608–1619.
[13] W.X. Tang, C.X. Zheng, Z.Y. Zhou, D.E. Jesson, J. Tersoff, Ga droplet surface dynamics during Langmuir evaporation of GaAs, IBM J. Res. Dev. 55 (2011) 10:1–10:7 https://doi.org/10.1147/JRD.2011.2158762.
[14] J. Tersoff, D.E. Jesson, W.X. Tang, Running droplets of gallium from evaporation of gallium arsenide, Science 324 (2009) 236–238 https://doi.org/10.1126/science.1169546.
[15] C.X. Zheng, J. Tersoff, W.X. Tang, A. Morreau, D.E. Jesson, Novel GaAs surface phases via direct control of chemical potential, Phys. Rev. B 93 (2016) 1–6 https://doi.org/10.1103/PhysRevB.93.195314.
[16] C. Zheng, W.X. Tang, D.E. Jesson, Planar regions of GaAs (001) prepared by Ga droplet motion, J. Vac. Sci. Technol. A 34 (2016) 043201 https://doi.org/10.1116/1.4948530.
[17] N. Koguchi, S. Takahashi, T. Chikyow, New MBE growth method for InSb quantum well boxes, J. Cryst. Growth 111 (1991) 688–692 https://doi.org/10.1016/0022-0248(91)91064-H.
[18] M. Yamagiwa, T. Mano, T. Kuroda, T. Tateno, K. Sakoda, G. Kido, N. Koguchi, F. Minami, Self-assembly of laterally aligned GaAs quantum dot pairs, Appl. Phys. Lett. 89 (2006) 113115 https://doi.org/10.1063/1.2354007.
[19] S. Huang, Z. Niu, Z. Fang, H. Ni, Z. Gong, J. Xia, Complex quantum ring structures formed by droplet epitaxy, Appl. Phys. Lett. 89 (2006) 031921 https://doi.org/10.1063/1.2234564.
[20] T. Mano, N. Koguchi, Nanometer-scale GaAs ring structure grown by droplet epitaxy, J. Cryst. Growth 278 (2005) 108–112 https://doi.org/10.1016/j.jcrysgro.2004.12.119.
[21] T. Mano, T. Kuroda, S. Sanguinetti, T. Ochiai, T. Tateno, J. Kim, T. Noda, M. Kawabe, K. Sakoda, G. Kido, N. Koguchi, Self-assembly of concentric quantum double rings, Nano. Lett. 5 (2005) 425–428 https://doi.org/10.1021/nl048192.
[22] C. Somaschini, S. Bietti, N. Koguchi, S. Sanguinetti, Shape control via surface reconstruction kinetics of droplet epitaxy nanostructures, Appl. Phys. Lett. 97 (2010) 203109 https://doi.org/10.1063/1.3511283.
[23] Z. Gong, Z.C. Niu, S.S. Huang, Z.D. Fang, B.Q. Sun, J.B. Xia, Formation of GaAs/AlGaAs and InGaAs/GaAs nanorings by droplet molecular-beam epitaxy, Appl. Phys. Lett. 87 (2005) 093116 https://doi.org/10.1063/1.2037193.
[24] C. Somaschini, S. Bietti, N. Koguchi, S. Sanguinetti, Fabrication of multiple concentric nano ring structures, Nano. Lett. 9 (2009) 3419–3424 https://doi.org/10.1021/nl901493f.
[25] A. Ohtake, Surface reconstructions on GaAs (001), Surf. Sci. Rep. 63 (2008) 295–327 https://doi.org/10.1016/j.surfrep.2008.03.001.
[26] L. Däweritz, Surface characterization by RHEED techniques during MBE growth of GaAs and $Al_xGa_{1-x}As$, Superlattice Microst. 9 (1991) 141–145 https://doi.org/10.1016/0749-6036(91)90270-2.
[27] For the Elmitec LEEM system, switching between different dark field images was achieved by changing the “Illum. Equal X/Y” deflectors inside the sector field. When the (0, 0) spot is selected, these two deflectors are set to zero.